

Arvind V. Gambheer, David R. Doelling, and Douglas A. Spangenberg
AS&M, Inc., Hampton, VA 23666

Patrick Minnis
NASA Langley Research Center, Hampton, VA 23666

1 INTRODUCTION

Precise knowledge of the radiation budget is absolutely necessary for understanding weather and the climate of the Earth. Accurate estimates of fluxes at the top of atmosphere (TOA) and emission at the surface are critical components of the radiation budget. At the Earth's surface, long wave (LW) emission is principally controlled by the surface radiating temperature or skin temperature (Ts). In addition, the land skin temperature is an important factor for agricultural monitoring and understanding of convective processes. Operational satellites estimate Ts using a parameterization based on infrared (IR) channels. Satellite-derived Ts products provide global coverage during clear-sky events. Infrared calibration, atmospheric water vapor absorption, surface emissivity and satellite viewing geometry affect the brightness temperature measured from the satellite. These factors must be taken into account to derive accurate values of Ts. The IR calibration on operational satellites has been shown to be reliable due to onboard blackbodies (Minnis et al. 2002). The relationship between the observed IR temperature T and Ts is a function of surface emissivity and atmospheric absorption. Viewing zenith angle effects are taken out using limb-darkening functions. However, it is also necessary to remove azimuthal dependent temperature variations.

Orientation of surface topography and vegetation with respect to the sun causes shadowing. Depending on the satellite viewing conditions, the satellite can either observe the colder shadowed portion of the surface or the warmer illuminated portion. Essentially shadows are observed in forward scatter conditions and the sunlit area in backscatter. Thus, colder brightness temperatures are observed in forward scatter and warmer temperatures in backscatter. Both IR window channel and LW channel radiances are affected, although it is less pronounced for broadband radiances due to atmospheric water vapor absorption. Minnis and Khaiyer (2000) examined the angular dependence of land skin temperature by using coincident clear-sky views from the Geostationary Operational Environmental Satellites, GOES-8, 9 and 10, which showed that

the instantaneous IR (10.8 μm) temperatures differed by as much as 6 K among the three satellites.

Minnis et al. (2004) examined, in detail, the azimuthal effects in LW due to shadowing by vegetation, topography, and clouds using Clouds and the Earth's Radiant Energy System (CERES) data. An azimuthal model was developed from CERES window channel radiances on the Tropical Rainfall Measuring Mission (TRMM) satellite and applied to coincident collocated Visible Infrared Scanner (VIRS) and geostationary 10.8 μm temperatures. It was shown that IR temperature prediction errors can be reduced by 35% or more over the full range of daylight viewing conditions if azimuthal corrections are applied.

The goal of this research is to identify and reduce the GOES-8 IR temperature biases, induced by a fixed geostationary position, during the course of a day. In this study, the same CERES LW window channel model is applied to GOES-8 IR temperatures during clear days over the Atmospheric Radiation Measurement-Southern Great Plains Central Facility (SCF). The model-adjusted and observed IR temperatures are compared with top-of-the-atmosphere (TOA) estimated temperatures derived from a radiative transfer algorithm based on the atmospheric profile and surface radiometer measurements. This algorithm can then be incorporated to derive more accurate Ts from real-time satellite operational products.

2 DATA

The Visible Infrared Solar-infrared Split-Window Technique (VISST) cloud and radiation retrieval algorithm was applied to half hourly GOES-8 4km pixels between March and December of 2000 over the ARM SGP (Minnis et al. 2002). All pixel-level data that lie within a 10-km radius centered at the ARM SGP CF site (36.62° N and 97.50° W) were averaged and are available at (http://www-angler.larc.nasa.gov/satimage/armsgp_groundsite.html). GOES-8 4-km IR temperatures were averaged in the same manner. VISST provides instantaneous cloud fractions based on a multi-channel cloud mask. Clear-sky conditions were identified whenever the cloud fraction was less than 5% and the clear-sky and total radiance were equal for both visible and IR channels. Snow periods were eliminated based on data from the NOAA operational daily snow cover analysis (<http://www.ssd.noaa.gov/PS/SNOW>), since measurements and cloud detection could be

*Corresponding author address: Arvind Gambheer, AS&M, Inc., 1 Enterprise Pkwy, Hampton, VA 23666. email: a.v.gambheer@larc.nasa.gov.

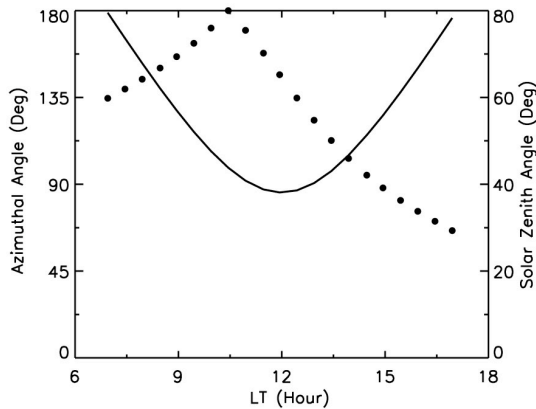


Fig. 1. The azimuthal (0° =forward scatter) and solar zenith angles at the SCF as a function of LT for September 26, 2000.

suspect in those conditions. To further ensure clear-sky conditions the standard deviation of T within the radii had to be less than 1° K. A minimum of 8 consecutive clear-sky observations were required for a day to be included in the dataset. There were a total of 54 days used in this study with an average of 11.4 measurements per day.

The Surface Infrared Radiation Station (SIRS) LW upwelling fluxes at the CF were used to estimate T_s . The 1-minute SIRS (sgpsirs1duttE13.c1 available at <http://www.arm.gov>) LW upwelling fluxes were averaged into 10-minute segments centered on the GOES-8 image times. T_s was computed using the Stephen Boltzman equation. No surface emissivity adjustment was made before applying the Stefan Boltzman equation, because T_s includes the surface emissivity. These skin temperatures were used to compute the TOA IR radiances using the correlated-k distribution method of Kratz (1995) weighted by the GOES-8 spectral response function. The correlated-k method computes the atmospheric transmissivity at any given view angle. The radiative transfer calculations are performed at 10° view angle increments and Gaussian weighted to obtain an equivalent GOES-8 IR estimated flux at the TOA (hereafter, TOA IR). Atmospheric profile data was taken from the Rapid Update Cycle (RUC) 40-km data set (version allruc40isob.c1 available at the ARM archive <http://www.arm.gov>). RUC, an operational mesoscale data assimilation and numerical forecast system run at the National Centers for Environmental Prediction (NCEP), is designed to provide frequently updated numerical forecast guidance (Benjamin et al. 2004). The RUC runs at the highest frequency of any forecast model at NCEP, assimilating observations to provide hourly profiles. The closest RUC hourly profile to the GOES-8 image was used in the correlated-k computations.

3 METHODOLOGY

GOES-8 (0° N, 75° W) views the SCF at a constant view angle of 48.65° . The solar zenith and relative azimuth angles for September 26, 2000 (near equinox)

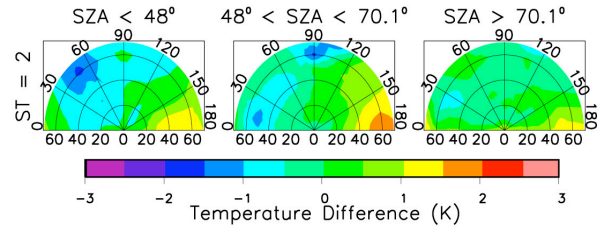


Fig. 2. Az-model-predicted temperature azimuthal differences as a function of solar zenith angle.

are shown in Fig. 1. The relative azimuth angle increases from 135° (forward scatter= 0°) at sunrise to 180° at 10.5 local time (LT) when the satellite and sun are aligned. The azimuth angles decrease until sunset. The SCF is in backscatter from sunrise until 15 LT and in forward scatter until sunset. The CERES TRMM window-channel-based LW azimuthal model (Az model) described in Minnis et al. (2004) is applied to the measured GOES-8 IR temperatures. The Az model corrects for limb-darkening and azimuthal variations. It returns an integrated flux from a given radiance similar to a shortwave bidirectional model. The Az model is a function of geo-type (surface type), surface height variability, and cloud amount. For clear-sky Az model computations at the SCF, a surface type of 2 (savanna), and the smallest surface height variability bin is used. The relative azimuthal temperature differences are shown in Fig. 2. The limb-darkening signal is greater than the azimuthal variation in most cases. For each 10° viewing zenith angle bin, the temperatures have been normalized to reveal the azimuthal signature. For all three solar zenith angle bins, forward scatter (azimuth angle= 0°) temperatures are less than those in backscatter. The greatest temperatures occur for azimuth angles greater than 150° , however, the minimum values can occur anywhere in the forward scatter section. The greatest azimuthal variation occurs in the $48\text{--}70^\circ$ solar zenith angle bin, where the combination of shadowing and solar flux is greatest.

The Az model temperature differences that can be expected for the viewing conditions at the CF as a function of LT are in shown in Fig. 3. The Az model predicts a maximum daily range of about 2° K. Since most of the azimuth angles throughout the day are in backscatter, except after 15 LT, there is an overall positive azimuthal temperature difference. Figure 3 also shows the observed GOES-8 IR temperatures. The large diurnal amplitude in the IR temperature can easily mask the azimuthal signal.

The estimated hemispheric TOA IR temperatures T_k derived using the correlated-k method and the SIRS-based T_s for September 26, 2000 are shown in Figure 4a. The morning points are in blue and the afternoon points are in red. T_s increases from sunrise until 13 LT and decreases until sunset. Only 12 of the points plotted in Fig. 3 are used in Fig. 4 due to the previously defined clear-sky restrictions. Atmospheric absorption reduced the TOA IR temperature by 2.18° K relative to T_s , based on RUC atmospheric profiles. The atmospheric component can be as great as 12.9° in the summer and

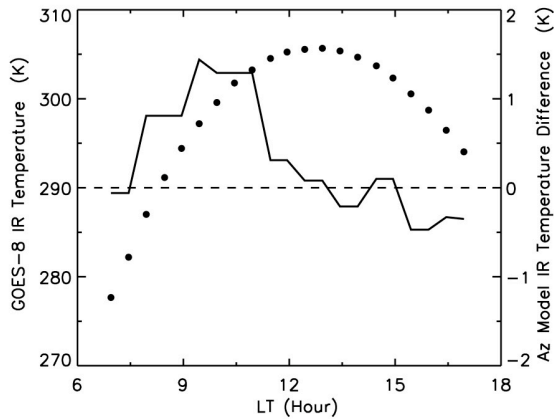


Fig. 3. The GOES-8 IR temperature observed and Az model predicted azimuthal temperature differences as a function of LT.

as low as 0.72° in winter. Although there is diurnal heating and cooling in the lower atmosphere, the precipitable water is relatively constant. The atmosphere introduces a slight AM-PM difference. A principal component linear regression (minimizing the distance to the regression line) has been applied to the measurements. Scatter about the regression line indicates diurnal variations in atmospheric absorption. The standard error or scatter about the line was 0.13° K. In this case, there is a slight AM-PM separation of points. To ensure that the AM-PM difference is not biased due to an unequal number of AM and PM points, the near sunrise or sunset points are eliminated until there is an equal number of points before and after 13 LT. Diurnal heating peaks at 13 LT (see Fig. 3).

Replacing the x-axis (Fig. 4b) with observed GOES-8 IR temperatures reveals a distinct separation of morning and afternoon points. The morning GOES-8 IR temperatures are greater than in the afternoon. This is in agreement with the Az model (see Fig 3). In this case the standard error is 0.84° K and is greater than the atmospheric component. It should be noted that the GOES-8 IR temperatures have not been corrected for flux. Since the view angle is constant, conversion to flux using a limb darkening function would not change the relative AM-PM difference (standard error), just the overall magnitude (location of the regression line). In Fig. 4c, the Az model has been applied to the GOES-8 IR temperatures and the AM-PM separation has been dramatically reduced. The standard error is 0.37° K, a 52% reduction, not including the atmospheric component. The Az model did not fully match the TOA IR temperature. No attempt has been made to tune the input to the correlated-k, since tuning might reduce the azimuthal signature.

4 RESULTS AND DISCUSSION

The methodology was applied to all clear days during 2000. The mean standard error was 0.30° , 0.64° ,

and 0.50° for T_s , GOES-8 IR, and the Az model IR compared with TOA IR, respectively. A 59% reduction in the standard error can be attributed to the Az model. The standard error was reduced for 42 of the 54 clear days, 78% of the time. Most of the Az model improvement occurred after June 6. During spring, 9 of the 13 clear days showed no improvement. For the rest of the year, 3 of 41 showed no improvement. Possible causes include plant height variations, oriented crops, vegetation or crop seasonal cycle, inversions, or measurement errors.

Perhaps, the atmospheric component could cause the spring discrepancy. AM-PM differences in the upper tropospheric humidity or strong inversions in the morning could mask the azimuthal signature, especially if there is a large path length or view angle. The greatest atmospheric component in AM-PM deviations occurs in summer and not in the spring. The annual and spring atmospheric component standard errors are 0.30° and 0.21° , respectively. The strongest clear-sky surface inversions occur at sunrise after which solar heating warms the surface. The inversion peak temperature must be greater than T_s in order to increase the TOA IR. For each clear-sky day, the inversion strength, defined as the difference between the inversion peak temperature and T_s , was computed from 12 UTC (5:30 LT) RUC profiles. During spring, 15% of the clear-sky days had an inversion strength greater than 2° compared to 34% for the remainder of the year. There was no significant correlation in the regression of daily inversion strength with Az model improvement. Thus, it does not appear that the inversions significantly alter the assumed azimuthal relationship in the clear-sky temperature.

To ensure that the Az model standard error reduction is due to a systematic AM-PM alignment, the daily percentage of morning points on the right of the regression line (see Fig 4) were computed. The same was done for afternoon points to the left of the regression line. The daily percentages were computed as a function of varying temperature distances away from the regression line. Table 1 shows the mean of the daily percentages. If 100% of the AM points are on the right side and 100% of the PM points are on the left side with a differential of 0.1° K, then the total AM-PM separation is 0.2° . During the AM, 80% of the GOES-8 IR points were consistently on the right side of the regression line and 77.1% of the PM points were on the left. This was expected, since the Az model predicted the greatest warming in the morning. More than 50% of the GOES-8 IR temperatures had an AM-PM separation of at least 0.4° and 25% of the points had at least 1.0° . The Az model should reduce the percentages at each of the AM-PM separation intervals. There is approximately a 15% reduction when applying the Az model in all cases. It is interesting that the atmospheric component AM-PM separation at 0° is similar to that of the GOES-8 IR. However, it is less than 50% of that of GOES-8, at an AM-PM of 0.4° separation. This indicates that most large AM-PM separations are a function of GOES-8 viewing geometry and not from the atmospheric component.

5 CONCLUSIONS AND FUTURE WORK

It has been shown that there is an azimuthal dependency in the GOES-8 IR temperatures due to diurnal variations in azimuth and solar angles. The Az model reduced the azimuthal dependency by 59%. The diurnal variation in atmospheric absorption tends to increase the T_k in the morning and reduce it in the evening, a behavior that is similar fashion to the azimuthal dependency. However, the atmospheric effect is smaller than the azimuthal dependency. An unknown factor reduces the effectiveness of the Az model during spring. Perhaps, the presence of soil moisture or dew would reverse the typical behavior by suppressing the surface heating during the morning as a result of evaporation. Wind variation could also be important factors in this comparison. The impact of such effects can be minimized by performing the comparisons using both GOES-8 and GOES-10 data simultaneously. Additionally, the SCF is in an area with little topography and short vegetation. Thus, the azimuthal signal is expected to be small. Baseline Surface Radiation Network sites with differing topography and vegetation types should be used to further test the Az model. After proper testing the Az model can be made operational to improve skin surface temperature retrievals.

6 ACKNOWLEDGEMENTS

The authors wish to thank Michele Nordeen for data processing. This research was funded by the Environmental Sciences Division of U.S. Department of

Energy through the Interagency Agreement DE-AI02-97ER6234.

7 REFERENCES

- Benjamin, S. G., et al., 2004: An Hourly Assimilation-Forecast Cycle: The RUC, *Mon. Wea. Rev.*, **132**, 495-518.
- Kratz, D. P., 1995: The Correlated k-Distribution Technique as Applied to the AVHRR Channels, *J. Quant. Spectrosc. Radiat. Transfer*, **53**, No. 5. 501-517.
- Minnis, P., Gambheer, A. V. and D. R. Doelling, 2004: Azimuthal anisotropy of longwave and infrared window radiances from the Clouds and the Earth's Radiant Energy System on the Tropical Rainfall Measuring Mission and Terra satellites, *J. Geophys. Res.*, **109**, D8, D08202 10.1029/2003JD004471
- Minnis, P. and M. M. Khaiyer, 2000: Anisotropy of land surface skin temperature derived from satellite data. *J. Appl. Meteorol.*, **39**, 1117-1129.
- Minnis, P., L. Nguyen, D.R. Doelling, D.F. Young, W.F. Miller, D.P. Kratz, 2002: Rapid Calibration of Operational and Research Meteorological Satellite Imagers. Part II: Comparison of Infrared Channels." *J. Atmos. Oceanic Technol.*, **19**, 1250-1266
- Minnis, P., et al., 2001: A near-real time method for deriving cloud and radiation properties from satellites for weather and climate studies. *Proc. AMS 11th Conf. Satellite Meteorology and Oceanography*, Madison, WI, Oct. 15-18, 477-480.

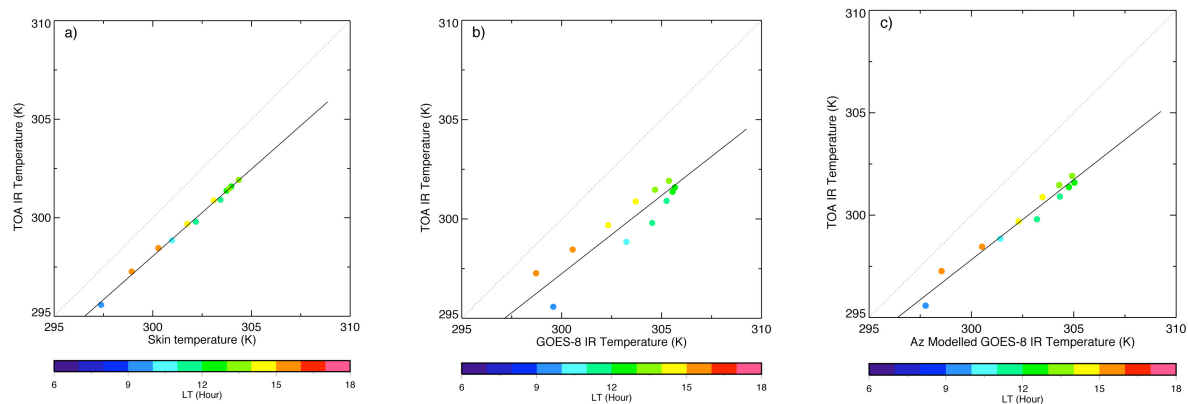


Fig. 4. (a) A scatter plot of half hourly T_s and TOA IR temperatures for September 26, 2000. Solid line is the regression line and the dotted line of agreement. (b) GOES-8 IR and TOA IR temperatures. (c). Az-modeled GOES-8 IR and TOA IR temperatures.

Table 1. The mean daily percentage of AM points to the right of the regression line and PM points to the left as a function of AM-PM separation.

| AM-PM Separation (K) | % AM on Right | | | % PM on Left | | |
|----------------------|---------------|------|----------|--------------|------|----------|
| | T_s | G-8 | Az Model | T_s | G-8 | Az Model |
| 0.0 | 81.3 | 80.6 | 68.0 | 78.5 | 77.1 | 65.2 |
| 0.2 | 46.2 | 69.2 | 54.5 | 49.7 | 68.6 | 47.3 |
| 0.4 | 29.6 | 54.3 | 39.0 | 29.1 | 59.5 | 40.1 |
| 1.0 | 7.5 | 26.6 | 15.1 | 9.0 | 33.4 | 16.7 |